Experimental verification of the Acuros XB and AAA dose calculation adjacent to heterogeneous media for IMRT and RapidArc of nasopharygeal carcinoma

Monica W. K. Kan[a)]
Department of Oncology, Princess Margaret Hospital, Kwai Chung, Hong Kong Special Administrative Region and Department of Physics and Materials Science, City University of Hong Kong, Tat Chee Avenue, Kowloon Tong, Hong Kong Special Administrative Region

Lucullus H. T. Leung and Ronald W. K. So
Department of Oncology, Princess Margaret Hospital, Kwai Chung, Hong Kong Special Administrative Region

Peter K. N. Yu
Department of Physics and Materials Science, City University of Hong Kong, Tat Chee Avenue, Kowloon Tong, Hong Kong Special Administrative Region

(Received 6 August 2012; revised 1 February 2013; accepted for publication 1 February 2013; published 27 February 2013)

Purpose: To compare the doses calculated by the Acuros XB (AXB) algorithm and analytical anisotropic algorithm (AAA) with experimentally measured data adjacent to and within heterogeneous medium using intensity modulated radiation therapy (IMRT) and RapidArc® (RA) volumetric arc therapy plans for nasopharygeal carcinoma (NPC).
Methods: Two-dimensional dose distribution immediately adjacent to both air and bone inserts of a rectangular tissue equivalent phantom irradiated using IMRT and RA plans for NPC cases were measured with GafChromic® EBT3 films. Doses near and within the nasopharygeal (NP) region of an anthropomorphic phantom containing heterogeneous medium were also measured with thermoluminescent dosimeters (TLD) and EBT3 films. The measured data were then compared with the data calculated by AAA and AXB. For AXB, dose calculations were performed using both dose-to-medium (AXB_D_m) and dose-to-water (AXB_D_w) options. Furthermore, target dose differences between AAA and AXB were analyzed for the corresponding real patients. The comparison of real patient plans was performed by stratifying the targets into components of different densities, including tissue, bone, and air.
Results: For the verification of planar dose distribution adjacent to air and bone using the rectangular phantom, the percentages of pixels that passed the gamma analysis with the ± 3%/3mm criteria were 98.7%, 99.5%, and 97.7% on the axial plane for AAA, AXB_D_m, and AXB_D_w, respectively, averaged over all IMRT and RA plans, while they were 97.6%, 98.2%, and 97.7%, respectively, on the coronal plane. For the verification of planar dose distribution within the NP region of the anthropomorphic phantom, the percentages of pixels that passed the gamma analysis with the ± 3%/3mm criteria were 95.1%, 91.3%, and 99.0% for AAA, AXB_D_m, and AXB_D_w, respectively, averaged over all IMRT and RA plans. Within the NP region where air and bone were present, the film measurements represented the dose close to unit density water in a heterogeneous medium, produced the best agreement with the AXB_D_w. For the verification of point doses within the target using TLD in the anthropomorphic phantom, the absolute percentage deviations between the calculated and measured data when averaged over all IMRT and RA plans were 1.8%, 1.7%, and 1.8% for AAA, AXB_D_m and AXB_D_w, respectively. From all the verification results, no significant difference was found between the IMRT and RA plans. The target dose analysis of the real patient plans showed that the discrepancies in mean doses to the PTV component in tissue among the three dose calculation options were within 2%, but up to about 4% in the bone content, with AXB_D_m giving the lowest values and AXB_D_w giving the highest values.
Conclusions: In general, the verification measurements demonstrated that both algorithms produced acceptable accuracy when compared to the measured data. GafChromic® film results indicated that AXB produced slightly better accuracy compared to AAA for dose calculation adjacent to and within the heterogeneous media. Users should be aware of the differences in calculated target doses between options AXB_D_m and AXB_D_w, especially in bone, for IMRT and RA in NPC cases.
 [http://dx.doi.org/10.1118/1.4792308]

Key words: Acuros XB algorithm, intensity modulated radiotherapy, RapidArc, heterogeneous media, GafChromic EBT3 film, anthropomorphic phantom

I. INTRODUCTION

Intensity modulated treatment techniques such as intensity-modulated radiotherapy (IMRT) and volumetric modulated-arc therapy (VMAT) are commonly used for the treatment of nasopharygeal carcinoma (NPC) due to the possibility of achieving better target coverage with lower doses to organs-at-risk (OAR) compared to three-dimensional conformal radiotherapy (3DCRT).[1–5] The capability of producing highly conformal plans to patients should be accomplished with accurate dose calculation, especially when strong variation of densities in small volumes exists.

A deterministic dose algorithm, the Acuros XB advanced dose calculation algorithm (AXB) has been implemented in the Eclipse treatment planning system (Varian Medical Systems, Palo Alto, CA) since 2010. It explicitly solves the linear Boltzmann transport equation (BTE) with numeric methods. The BTE is the governing equation that describes the macroscopic behavior of radiation particles as they travel through and interact with matter. Similar to the traditional Monte Carlo method, it allows for accurate modeling of dose deposition in heterogeneous media.

Several investigations have been performed to compare the dose calculation accuracy of the newly released AXB against Monte Carlo simulations and commonly used superposition-convolution algorithms such as analytical anisotropic algorithm (AAA) and collapsed-cone convolution (CCC) method in homogeneous water and heterogeneous multilayer slab phantoms using single fields.[6–10] The media involved in the previous studies included tissue, normal lung, low-density lung, air, and bone. In general, the results indicated good agreement between AXB and Monte Carlo calculations, and AXB was considerably more accurate than superposition-convolution algorithms. Vassiliev *et al.*[6] assessed the performance of AXB from a pair of tangential fields in an anthropomorphic phantom for a breast case and found excellent agreement between AXB and Monte Carlo simulations.

Relatively few experimental verifications with clinical set-up fields were found. Han *et al.*[11] have reported verification results of AXB for IMRT and VMAT using the Radiological Physics Center head and neck (RPC H&N) phantom. Predicted dose distributions by AAA and AXB with both dose-to-medium (AXB_D_m) as well as dose-to-water (AXB_D_w) options were compared to doses measured using thermoluminescent dosimeters (TLDs) and GafChromic® EBT2 film. They observed that AXB_D_m produced slightly better agreement with measurement results than AXB_D_w and AAA. The RPC H&N phantom was made primarily of water-equivalent materials. Only very small air gaps existed near the TLD and film insert and their effects to the dose calculation were negligible. Thus, the effects from heterogeneities could not be fully investigated. Our previous study, which compared the performance of AXB and AAA using TLD measurement at and near air/tissue interfaces in an anthropomorphic phantom using intensity modulated stereotactic set-up fields found better agreement between AXB_D_m and measurement compared to AAA.[12] However, the dose variation effect due to electronic disequilibrium for stereotactic fields was not the same as that for IMRT and VMAT fields in primary treatments due to the differences in field segment sizes, the target volumes being irradiated, the complexity of beam modulation, and beam directions. The main aim of this study was to perform verification of AXB_D_m, AXB_D_w and AAA dose calculations adjacent to and within heterogeneous medium with both air and bone for IMRT and RapidArc (RA) plans in NPC. The accuracy of the two-dimensional (2D) dose distribution adjacent to both air and bone inserts of a simple geometric phantom was validated with absolute dose gamma analysis using the newly released GafChromic® EBT3 film. The planar dose distribution near and within the nasopharygeal (NP) region of an anthropomorphic phantom containing heterogeneous medium was also measured using the EBT3 film. Besides, the accuracy of point doses near and adjacent to air and bone was verified in the anthropomorphic phantom using TLDs. This phantom was modified by the authors to accommodate TLD chips adjacent to and near air or bony structures in the head and neck region.

To further understand the differences in the calculated dose distributions between AAA and AXB, as well as between dose-to-medium and dose-to-water options of the AXB in materials of different densities, the target dose differences among AAA, AXB_D_m, and AXB_D_w were analyzed for the corresponding real patients. The comparison of real patient plans was performed by stratifying the targets into components of different densities, including tissue, bone, and air. The mean doses to the planning target volumes (PTV) divided into components of bone, air, tissue (the remaining tissue after excluding air and bone), tissue that was 3 mm adjacent to bone and tissue that was 3 mm adjacent to air for the IMRT and RA plans predicted by AAA, AXB_D_m, and AXB_D_w were calculated and compared. This might also help determine the correlation between the clinical planning results and the verification results.

II. MATERIALS AND METHODS

II.A. Phantoms for experimental verification

The head and neck cube of the commercially available Scanditronix Wellhofer I'mRT RW3 phantom (IBA Dosimetry, Uppsala, Sweden) containing air cavity and bone insert was used for verification of 2D distribution adjacent to heterogeneous medium. The dimension of the head and neck cube was 18 × 18 × 18 cm, in which the volume for accommodating phantom slabs was 16 × 16 × 16 cm, with 1 m edge on each side. An air cavity of 4 × 4 × 16 cm and a cylindrical bone insert of 16 cm length and 0.8 cm diameter with a physical density of 1.64 g/cm^3 were used as shown in Fig. 1. Figure 1(a) shows the coronal view of the phantom, with the arrow indicating where the film was inserted adjacent to the heterogeneous media. Figure 1(b) shows the actual geometrical set-up of the cube relative to the radiation field when the film was placed on the axial plane. In order to take into account the Hounsfield unit (HU) of the film material in the CT scan during automatic material assignment for AXB

FIG. 1. The (a) coronal view of head and neck cube of the Scanditronix Wellhofer I'mRT phantom containing air cavity and bone insert, and its position relative to the radiation beam during measurement of planar dose distribution on (b) axial plane and (c) coronal plane.

dose calculation and minimize the partial volume effect on the CT image, an extra 2 mm thick of film material (created using discarded GafChromic films) was placed adjacent to the film for actual measurement as shown in Fig. 1(a). Each film was cut to 16 × 9 cm and placed at the center of the axial plane. Perspex material of 2 mm thickness was precisely cut to fill up the rest of the spaces that was not occupied by films. In addition, to repeat similar measurements of planar dose distribution on the coronal plane, the cube was rotated by 90° as shown in Fig. 1(c). The film was placed on the center of the coronal plane immediately below the air cavity and bone inserts.

The head and shoulder region of an anthropomorphic phantom (the RANDO phantom, The Phantom Laboratory, Salem, NY) as shown in Fig. 2(a) was used for verification of point doses by TLD measurements and planar dose distributions near the NP region by film measurements. The phantom included bone, lung, and soft tissue compositions formulated for accurate simulation for therapy energies. The whole phantom was divided into 26 sections, each with 25 mm thickness, and only the first 11 phantom sections from the top of the head down to the shoulder region were used for the current investigation. For measurement of planar dose distributions, one film at a time was sandwiched between two of the phantom

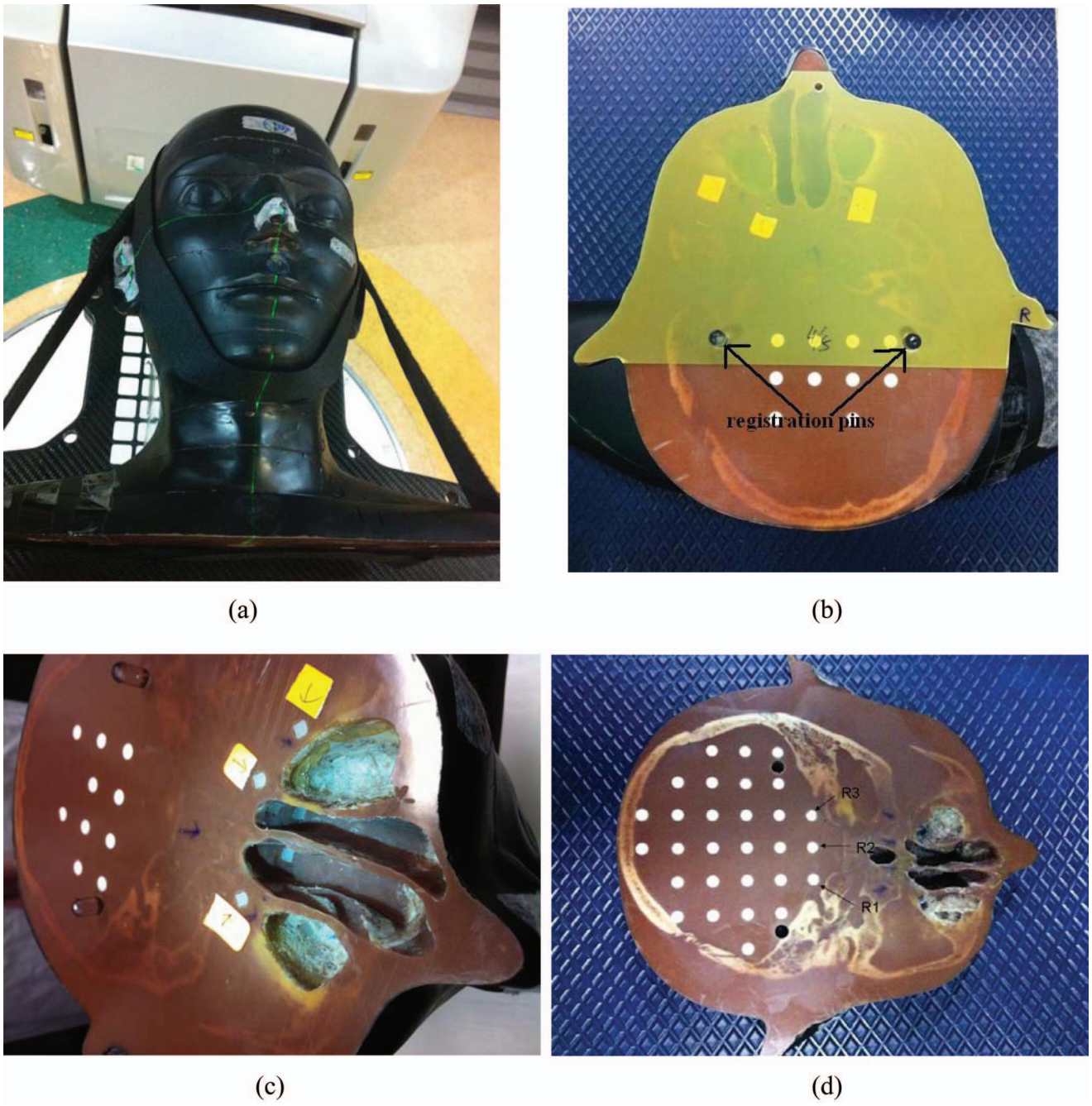

FIG. 2. (a) Head and shoulder region of the anthropomorphic phantom for TLD and film verification. (b) The position of the EBT3 film for measurement of planar dose distribution near the NP region. (c)The position of seven TLD chips near the nasal cavities and maxillary sinuses. (d) The position of the three TLD chips near the brain stem.

sections. The position of measurement was chosen to be near the NP region within tissue, bone, and air cavity. The film was cut carefully following the contour of the chosen phantom section. The thickness of the film was about 0.2 mm, which was much smaller than the CT scan slice. Direct CT simulation of the thin film within the NP region was not performed. Therefore, the film should only represent doses close to water density in heterogeneous medium. Each section of the phantom consisted of two registration pins that held phantom sections together in proper alignment. In order to anchor the film firmly and reproducibly between the phantom sections, two 6 mm diameter circular holes that precisely matched the positions and size of the registration pins to within 0.1 mm were cut from the films, as shown in Fig. 2(b). Since the regions at and near the registration pins would produce inaccurate results for the gamma analysis, only the region anterior to the pins where most of the air and bone were present was included in the region of interest (ROI).

For TLD measurement, only a few TLD recesses of the original phantom could be found near bone/tissue interfaces and almost none near air/tissue interface. The phantom was therefore modified by creating some TLD recesses near

TABLE I. Distribution of TLD chips in the anthropomorphic phantom.

TLD position no.	Position in the anthropomorphic phantom
T1, T2	Near oropharynx
T3–T5	At air/tissue interface of oral cavity
T6, T7	At air/tissue interface of nasal cavity
T8, T9	At air/bone interface of nasal cavity
T10	Near bone/tissue interface, close to nasal cavity and maxillary sinus
T11, T12	Near air/tissue interface of maxillary sinus
R1–R3	Near brain stem
R4–R6	Near posterior region of brain stem

heterogeneous interfaces and air cavities near the NP region mimicking that of a typical real patient. Two TLD chips were placed in the tissue near the oropharynx. Three of them were placed near the air/tissue interface of the oral cavity. Seven of them were placed near the nasal cavities and maxillary sinuses, some near air/tissue interfaces and some near bone/tissue interface as shown in Fig. 2(c). Besides, six TLD chips were placed near the brain stem outside the target volume to represent verification of doses in OAR, three of which were shown in Fig. 2(d). Table I summarizes the distribution of the TLD positions in the phantom.

II.B. Treatment planning, dose calculation, and delivery

The CT scans of both the head and neck cube and the anthropomorphic phantom were performed with a GE LightSpeed RT 16-multislice CT simulator (GE Healthcare, Waukesha, WI). Although the slice thickness for the NPC planning of our routine clinical cases was 2.5 mm, a thinner slice thickness of 1.25 mm was used for the verification phantom scan for better visualization and sampling of the HU values of film and TLD chips.

Three patients with NPC who were previously treated with RA plans were replanned with sliding window IMRT. All plans were generated using 6 MV beam and modulated with 120 multileaf collimator (MLC) from a linear accelerator (Clinac 23EX, Varian Medical Systems). They were created with the Eclipse version 10.0 (Varian Medical Systems, Inc., Palo Alto). IMRT plans were created using nine fields that were evenly distributed in coplanar beam directions. The RA plans were created using two complete arcs, each with 358° arc length plus one partial arc (from gantry angle of 240° to 120° in the clockwise direction). The couch angles of all arcs were 0°. Nonzero collimator angles were used for all RA plans to reduce the tongue and groove effect. Three planning target volumes were defined for each patient, with 7000 cGy prescribed to PTV_{GTV} (PTV including the gross target volume), 6000 cGy to PTV_{H_CTV} (PTV including the high risk clinical target volume), and 5400 cGy to PTV_{L_CTV} (PTV including the low risk target volume). Different dose levels to PTVs were achieved using simultaneous integrated boost technique (SIB). The optimization goal was to ensure at least 95% of the PTVs and 100% of the GTV to receive the prescribed dose, and no more than 5% of the PTV_{GTV} would receive 107% of the prescribed dose while minimizing the doses to organs at risk (OARs). Optimization and dose calculation were originally performed based on AAA 10.0.28 with 2.5 mm grid resolution. The planning parameters of all six plans including beam angles, MLC leaf settings, jaws sizes, and monitor units (MU) were transferred to the CT images of the verification phantoms and then recalculated using AAA, AXB_D_m, and AXB_D_w of version 10.0.28.

AAA originally developed based on the superposition-convolution method was implemented to replace the pencil beam model for more accurate dose calculation in heterogeneous media. It uses Monte Carlo derived kernels and provides a better modeling of the dose deposition in comparison to pencil beam model. Tissue inhomogeneities are taken into account by using radiologic scaling of the dose deposition functions in the beamlet direction and electron-density-based scaling of the scatter kernels in the lateral directions. Detailed description of the algorithm can be found in the papers by Ulmer *et al.*[13] and Fogliata *et al.*[14]

Two options of dose reporting modes were available in AXB, dose-to-water, D_w, and dose-to-medium, D_m. Both options calculate dose considering the elemental composition of each material in which particles are transported. The only difference is in the postprocessing step, in which D_w is obtained by rescaling D_m using the stopping power ratio of water-to-medium. To account for material properties of the interested media, tissue segmentation is based on density ranges related to HU from the CT images, and for each tissue the specific chemical composition is considered based on ICRP 23 report.[15] Detailed description of the algorithm can be found in several previous publications.[6–10]

The isocenter position in the anthropomorphic phantom was selected to be similar to that of the corresponding real patient. The isocenter position in the head and neck cube was chosen such that high dose regions covered the air and bone insert, as well as the film.

II.C. Film and TLD measurement

The GafChromic EBT3 films (Ashland, Specialty Ingredients, NJ) were used for the measurement of 2D dose distribution. There are some improvements in the design of the newly released EBT3 films when compared to EBT2 films. The 28 μm of active layer is sandwiched between layers of Matte Polyester substrate that negates Newton's rings. Its symmetric structure design allows the possibility of scanning the film from either side. All film analyses described in this study were performed with the Epson V700 (Epson, Suwa, Nagano) flat bed scanner using the response in red color channel. To minimize the warming up effects of the scanner lamp, at least seven successive scans for warm-up were performed at the beginning of each measurement series. The scanner was configured to scan with 150 dpi (0.17 mm/pixel). Several tests were performed regarding the performance of the film before they were used for the actual planar dose verifications. The reproducibility of the scanner was found by repeated

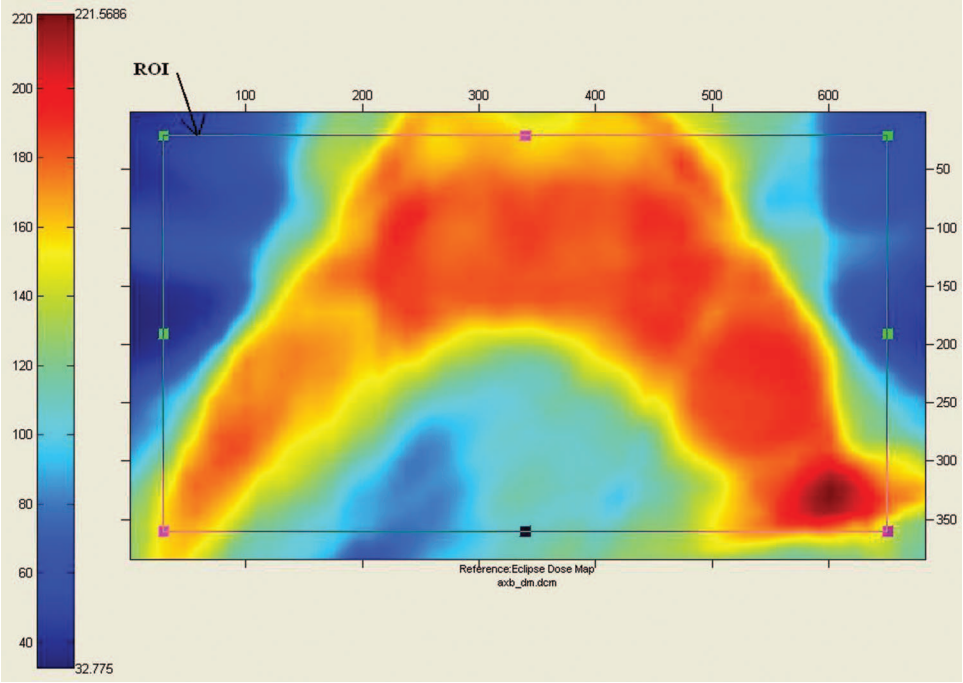

FIG. 3. The rectangular ROI of a typical planar distribution for the film analysis using the head and neck cube.

scanning of the same film irradiated to 100 cGy for 20 times. The relative standard deviation (RSD) of scanned values was found to be 0.4%. The intrasheet uniformity was determined by cutting small pieces of 5 × 5 cm films at different positions from the same sheet exposed to 100 cGy. The variation of scanned values at different positions was within ± 0.5%. The homogeneity among several films (interfilm uniformity) of the same batch was found by exposing small pieces of films that were cut from three different sheets exposed to the same dose. The variation of scanned values among different films was found to be within ± 0.5%. For determination of the influence of the film orientation during scanning, four pieces of films exposed from 25 to 400 cGy were scanned in landscape, portrait directions and also on both sides. The averaged difference in the scanned values between portrait and landscape scan was 12%, while that between both sides was only 0.5%. The dose calibration curves were determined by exposing small pieces of films (5 × 5 cm) to seven different doses ranged from 25 to 250 cGy. The films for measuring all planar dose distribution of the head and neck cube were cut from the original sheets of the same batch. All films were scanned on the day following the irradiations. Each piece of film was scanned near the center of the scanner in the landscape orientation of the same side facing upwards. The data were analyzed using the Rochester Institute of Technology (RIT) software version 4.3 (Radiological Imaging Technology, Inc., Colorado Spring). The dose to optical density calibration curve was used to convert the measured planar film image to a dose image which was then compared to the IMRT plan or RA plan in the film plane. Gamma index analysis with the test criteria of 3% dose agreement within a distance to agreement (DTA) of 3 mm (3%/3 mm), and also 2% dose agreement within a DTA of 2 mm (2%/2 mm) were performed. A rectangular ROI for the film analysis using the head and neck cube was defined to include mainly the high dose region near the PTV together with the nearby dose falloff gradient, with a typical example shown in Fig. 3. It mainly included regions adjacent to both air and bone inserts. A gamma value of larger than 1 would be assigned for points failing the gamma criterion within the ROI. The percentage of points with gamma >1 was assessed as a measure of disagreement between measurements and calculations. To reduce statistical uncertainty, the measurement for each plan was repeated three times. Three IMRT plans and three RA plans were validated. Planar dose distributions on both axial and coronal planes adjacent to air and bone inserts were measured. The confidence limit, CL, used in the TG 119 study to define the acceptability of the results was also estimated in this film study.[16] CL is defined as the sum of the absolute value of the average difference and the standard deviation of the differences multiplied by a factor of 1.96 (CL = |mean|+ 1.96 σ). Almost exactly the same procedures were used for the film analysis in the anthropomorphic phantom. Planar dose distribution measurements were only performed on the axial plane, as the phantom did not allow the placement of film on the coronal plane. The ROI for gamma analysis was chosen to exclude points near the edge of the contour, and those at and posterior to the two registration pins. As a result, the ROI mainly included those high dose regions near the target volumes together with dose falloff near the brain stem.

Doses at 18 different reference points were measured by LiF TLD-100 (3 × 1 × 1 mm) for three IMRT plans and three RA plans in the head and shoulder region of the anthropomorphic phantom. All TLDs were annealed at 400 °C

for 1 h and 100 °C for 2 h before irradiation. The whole set of TLDs were irradiated with a known dose of 100 cGy using 10 × 10 cm 6 MV x-ray beam before the actual measurement. To remove the short half-life peaks, the irradiated TLDs were preheated at 100 °C for 10 min. They were read by the Harshaw Model 5500 reader (Thermo Electron Corporation, Ohio). The precision of TLD measurement could be reduced to about 2% by assigning individual sensitivity value to each chip of one set.[17,18] The whole set of TLD chips were irradiated using 6 MV beam to 100 cGy in solid water at a depth of 5 cm. From the calibration, each chip was assigned a sensitivity value which related its individual dose response to the mean dose response of the set. The sensitivity value was then taken as the running average of three calibrations. A recalibration of individual sensitivity of each chip of the whole set was performed after one month. Based on comparisons between repeated irradiations of the TLD chips in a constant setup to a known dose, the precision of TLD measurement was 2.3%. During the actual measurement, the phantom for each plan was repeated three times and the averaged values were taken to reduce statistical errors. The originally prescribed dose to the target volume was 7000 cGy in 35 fractions (200 cGy per fraction). In order to perform all the measurement within the linear dose response range of the TLD-100 chips, the prescribed dose was reduced to 90 cGy per fraction. All TLDs were put to the reference positions and CT scanned together with the phantom. All the TLD chips selected for dose verification were clearly seen from the CT images. All TLDs within the target were at positions of uniform doses. High dose gradient was avoided, so that the influence of set-up error on measured doses could be minimized during delivery. However, those TLDs for measuring the doses near OAR were at regions of relatively higher dose gradient. Each TLD chip was manually contoured in the planning CT images and the calculated mean dose of each was taken as the calculated doses.

II.D. PTV analysis for real patients

For the six real patient plans (three IMRT and three RA plans) described in Secs. II.B and II.C, the effect of heterogeneity on the dose calculations among AAA, AXB_D_m, and AXB_D_w was also further studied by analyzing the PTV doses. Since PTV_{GTV} included the largest proportion of bone and air compared to the other PTVs with lower dose prescription, analysis was confined to PTV_{GTV} in the current study. The air cavities and bony structures in PTV_{GTV} were contoured separately as PTV_{GTV}_air and PTV_{GTV}_bone, as shown in Figs. 4(a) and 4(b). The rest of the volumes other than bone and air were contoured as PTV_{GTV}_tissue, as shown in Fig. 4(c). Besides, the tissue that was 3 mm adjacent to air and bone, was contoured as separate organ, i.e., PTV_{GTV}_adj air and PTV_{GTV}_adj bone, respectively, as shown in Figs. 4(d) and 4(e). For the originally contoured PTV_{GTV} and those corresponding stratified components, mean doses were calculated and compared.

III. RESULTS

III.A. Verification of planar dose with EBT3 films in head and neck cube

Table II summarizes the results of the gamma evaluations for the three clinical NPC cases using IMRT and RA plans on the axial plane using the head and neck cube. It can be seen that good agreements were found for the planar dose comparison with the 3%/3 mm criteria between measurements and all three calculation options. The percentage of pixels failing the 3%/3 mm criteria within the rectangular ROI averaged over all measurements and all plans was 1.3 ± 1.5%, 0.5 ± 0.5%, and 2.3 ± 2.3% for AAA, AXB_D_m, and AXB_D_w, respectively. The estimated CL values of both AAA and AXB were well within the action levels recommended by TG 119. When the restriction of gamma evaluation was raised to the criteria of 2%/2 mm, the percentage of pixels failing the gamma index increased to 7.4 ± 6.0%, 4.2 ± 3.5%, and 9.6 ± 9.1% for AAA, AXB_D_m, and AXB_D_w, respectively. Looking at the gamma evaluation with both 3%/3 mm and 2%/2 mm criteria for each individual plan, the planar dose distribution calculated by AXB_D_m showed the best agreement with the measured dose distribution by films for all plans except the RA plan for case 3. However, for this case the passing rates among the three calculation options were close to each other. At least it could be concluded that the passing rates for AXB_D_m for this plan was as good as the other two options.

The absolute values of averaged percentage dose differences between the calculated and measured values within the ROI averaged over all measurements and all plans were within 3% for the three calculation options. It was 1.8 ± 1.5%, 1.2 ± 1.8%, and 2.2 ± 1.8% for AAA, AXB_D_m, and AXB_D_w, respectively. For most of the plans, the averaged doses predicted using AAA and AXB_D_w were slightly higher than the measured doses. It was up to about 3% for AAA and 4% for AXB_D_w. The average doses predicted using AXB_D_m were lower than the measured values for some cases (the IMRT plans of cases 1 and 2, the RA plan of case 3), while higher than the measured values for the rest of the cases. It could also be observed that AXB_D_m predicted lower average planar doses than the other two options.

Figures 5(a)–5(c) show the spatial distribution of the gamma analyses with 3%/3 mm criterion for one film irradiated using the IMRT plan of case 1. By comparing the figures, it can be seen that the area of dose differences between measured doses and calculated doses using AXB_D_m was relatively smaller than that when the doses were calculated with AAA and AXB_D_w.

Table III summarizes the results of the gamma evaluations on the coronal plane using the head and neck cube. Good agreements were also found for the comparison using the 3%/3 mm criteria between measurements and all three calculation options. The percentage of pixels failing the 3%/3 mm criteria within the ROI averaged over all measurements and all plans was within 3% for all three calculation options. The estimated CL values were all well within the TG 119 recommended action levels, with a slightly higher passing rate

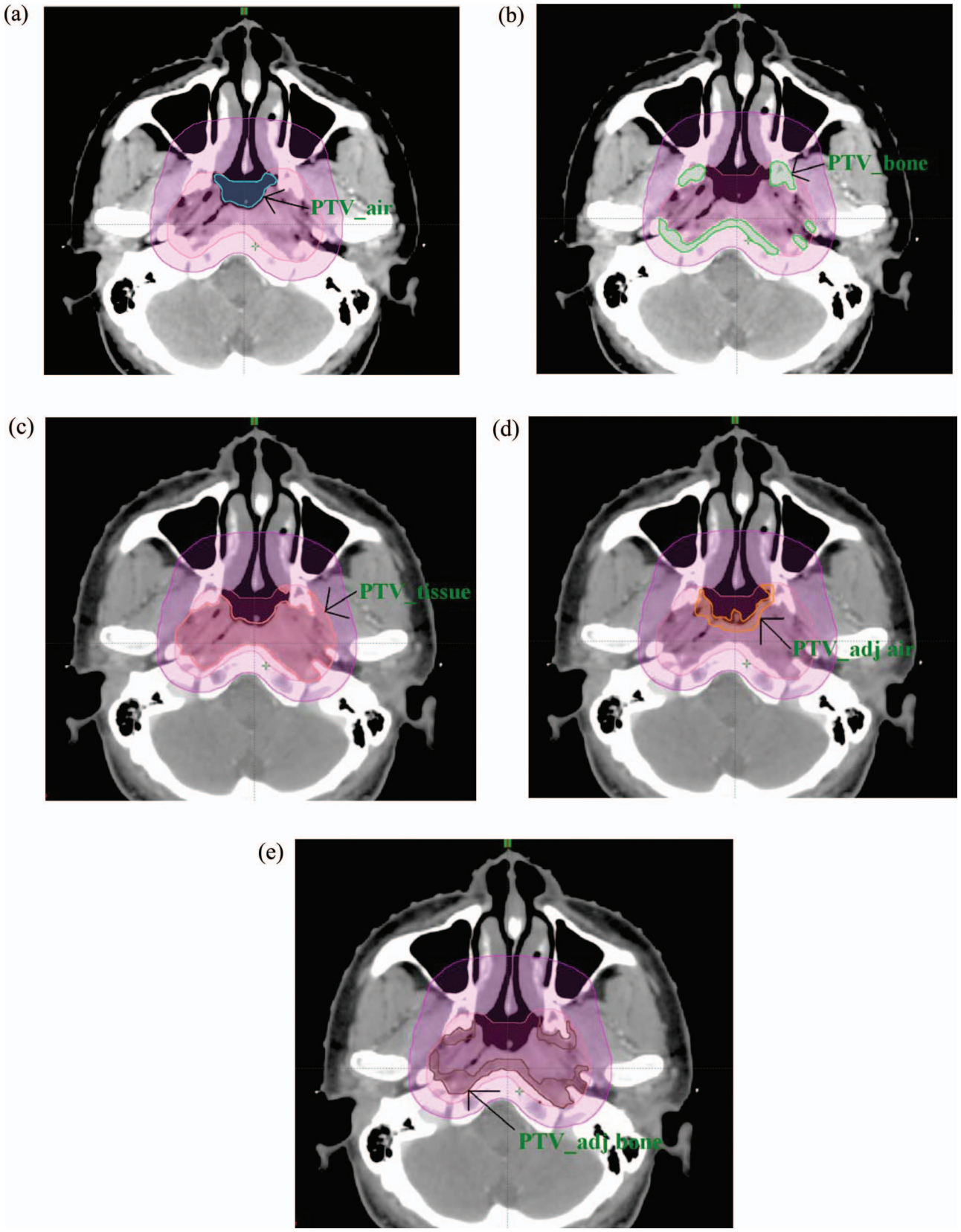

FIG. 4. One of the axial images of a NPC patient demonstrating the stratification of PTV_{GTV} in (a) air, (b) bone, (c) tissue, (d) tissue that was 3 mm adjacent to air and (e) tissue that was 3 mm adjacent to bone.

TABLE II. The averaged results of the gamma evaluations for the IMRT plans and RA plans over three repeated measurements on the axial plane using the head and neck cube.

IMRT	Dose calculation	Percentage of pixels with gamma > 1		Average dose difference within the ROI (%) (calculated data − measured data)
		3 mm/3%	2 mm/2%	%Δ
Case 1	AAA	0.4 ± 0.2	3.8 ± 1.3	0.9 ± 0.1
	AXB_Dm	0.2 ± 0.1	1.9 ± 0.5	−0.2 ± 0.2
	AXB_Dw	0.6 ± 0.8	3.3 ± 1.9	1.3 ± 0.2
Case 2	AAA	0.2 ± 0.3	2.6 ± 1.6	1.3 ± 0.8
	AXB_Dm	0.0 ± 0.0	1.9 ± 2.4	−0.1 ± 0.3
	AXB_Dw	0.5 ± 0.5	2.2 ± 1.7	1.4 ± 1.0
Case 3	AAA	1.8 ± 2.2	8.1 ± 6.8	2.1 ± 1.0
	AXB_Dm	1.0 ± 1.0	5.2 ± 4.1	0.8 ± 1.0
	AXB_Dw	2.4 ± 3.5	8.9 ± 8.0	2.3 ± 1.0
RA	Dose calculation	Percentage of pixels with gamma > 1		Average dose difference within the ROI (%) (calculated data − measured data)
		3 mm/3%	2 mm/2%	%Δ
Case 1	AAA	1.2 ± 0.3	10.8 ± 0.8	3.3 ± 0.2
	AXB_Dm	0.2 ± 0.1	3.6 ± 0.5	2.4 ± 0.2
	AXB_Dw	4.2 ± 1.5	18.4 ± 2.0	4.0 ± 0.3
Case 2	AAA	4.1 ± 3.6	15.2 ± 8.9	3.2 ± 1.2
	AXB_Dm	1.3 ± 1.4	8.0 ± 5.8	2.5 ± 1.2
	AXB_Dw	5.9 ± 5.1	20.3 ± 12.2	4.0 ± 1.2
Case 3	AAA	0.3 ± 0.2	4.4 ± 1.8	−0.2 ± 2.2
	AXB_Dm	0.5 ± 0.6	4.9 ± 3.3	−0.9 ± 2.2
	AXB_Dw	0.4 ± 0.4	4.4 ± 3.8	0.6 ± 2.2
		Overall combined (all IMRT and RA plans)		
		3 mm/3%		Confidence limit, CL (|mean|+ 1.96σ)
	AAA	1.3 ± 1.5		4.3 (95.7% passing)
	AXB_Dm	0.5 ± 0.5		1.5 (98.5% passing)
	AXB_Dw	2.3 ± 2.3		6.8 (93.2% passing)

observed for AXB_D_m when compared to that of AAA and AXB_D_w.

III.B. Verification of planar dose with EBT3 films in anthropomorphic phantom

Table IV summarizes the averaged results of the gamma evaluations for film measurement within the NP region of the head and shoulder anthropomorphic phantom. The percentage of pixels failing the 3%/3 mm criteria averaged for all plans was 4.9 ± 3.1%, 8.7 ± 3.6%, and 1.0 ± 0.6% for AAA, AXB_D_m, and AXB_D_w, respectively. When the restriction of gamma evaluation was raised to the criteria of 2%/2 mm, the percentage of pixels failing the gamma index increased to 18.0 ± 5.9%, 22.0 ± 5.6%, and 6.2 ± 3.0% for AAA, AXB_D_m, and AXB_D_w, respectively. Consistently better agreement can be found between measurements and AXB_D_w than AAA and AXB_D_m. The comparison results were similar between IMRT and RA plans. The estimated CL values of both AAA and AXB_D_w were within the action levels recommended by TG 119. The relatively larger disagreement between AXB_D_m and the measured data was mainly due to the fact that the measured doses by tissue equivalent film only represented doses close to unit water density within the heterogeneous medium.

III.C. Verification of point dose with TLD

The results of the anthropomorphic head and shoulder phantom verification measurement for the 12 points at/near heterogeneous interfaces within the target of IMRT plans and RA plans are shown in Tables V and VI, respectively. The average SD of all measurement points was 1.2%, with a range from 0.2% to 3.3%, showing reasonable consistency of the measurements. The dose variation of the algorithms came from the standard deviation of the predicted doses within the volume of each contoured TLD chip. Such variation was mostly within 1% inside the target. The absolute discrepancy

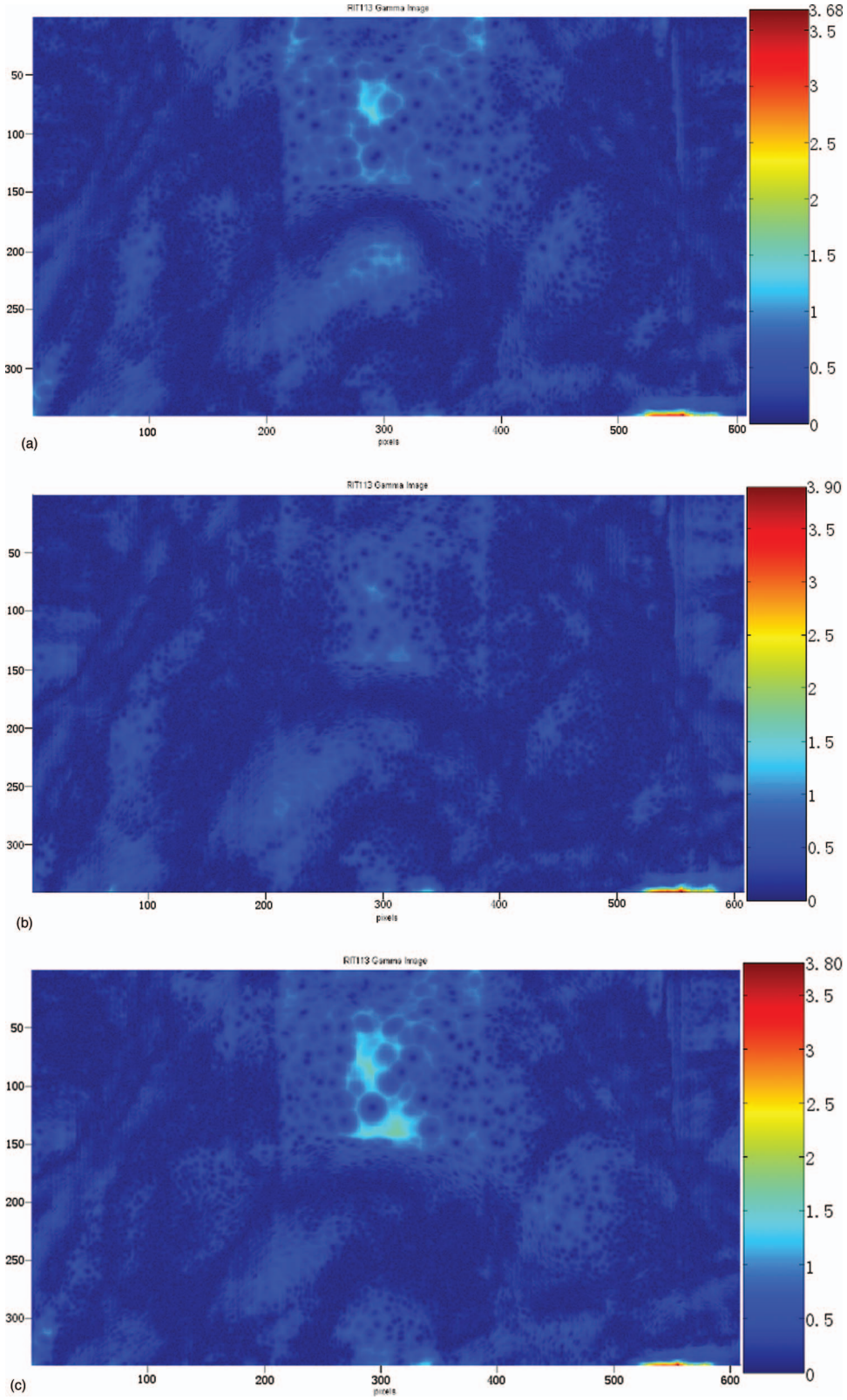

FIG. 5. The spatial distribution of the gamma analyses with 3%/3 mm criterion for one film irradiated using the IMRT plan of case 1 when compared to those calculated by (a) AAA, (b) AXB_D_m, and (c) AXB_D_w.

TABLE III. The averaged results of the gamma evaluations for the IMRT plans and RA plans over three repeated measurements on the coronal plane using the head and neck cube.

IMRT	Dose calculation	Percentage of pixels with gamma > 1		Average dose difference within the ROI (%) (calculated data − measured data)
		3 mm/3%	2 mm/2%	%Δ
Case 1	AAA	1.8 ± 1.6	9.3 ± 5.8	1.8 ± 1.0
	AXB_Dm	1.6 ± 1.5	7.3 ± 6.5	1.1 ± 1.0
	AXB_Dw	3.8 ± 3.0	15.8 ± 8.3	2.9 ± 1.0
Case 2	AAA	2.2 ± 1.3	7.3 ± 2.6	−1.3 ± 1.0
	AXB_Dm	1.5 ± 1.4	8.3 ± 4.5	−1.9 ± 0.9
	AXB_Dw	0.6 ± 0.6	4.8 ± 3.8	0.0 ± 0.9
Case 3	AAA	0.7 ± 0.4	3.5 ± 0.9	−0.2 ± 0.3
	AXB_Dm	0.1 ± 0.1	2.2 ± 2.1	−0.4 ± 0.7
	AXB_Dw	0.2 ± 0.1	3.3 ± 1.0	1.2 ± 0.3
RA	Dose calculation	Percentage of pixels with gamma > 1		Average dose difference within the ROI (%) (calculated data − measured data)
		3 mm/3%	2 mm/2%	%Δ
Case 1	AAA	8.0 ± 1.3	17.5 ± 5.5	1.8 ± 0.4
	AXB_Dm	4.3 ± 3.0	12.7 ± 6.0	0.4 ± 0.4
	AXB_Dw	6.0 ± 0.9	15.1 ± 4.7	2.2 ± 0.4
Case 2	AAA	1.2 ± 0.9	4.2 ± 2.1	1.3 ± 1.7
	AXB_Dm	1.5 ± 1.9	5.0 ± 2.9	0.5 ± 1.6
	AXB_Dw	2.1 ± 2.2	5.6 ± 4.5	2.1 ± 1.7
Case 3	AAA	0.4 ± 0.2	2.6 ± 0.6	0.4 ± 1.1
	AXB_Dm	1.5 ± 0.8	4.2 ± 2.8	1.2 ± 1.1
	AXB_Dw	1.4 ± 0.7	5.3 ± 1.6	1.9 ± 1.2
		Overall combined (all IMRT and RA plans)		
		3 mm/3%		Confidence limit, CL (|mean|+ 1.96σ)
	AAA	2.4 ± 2.8		7.9 (92.1% passing)
	AXB_Dm	1.8 ± 1.4		4.5 (95.5% passing)
	AXB_Dw	2.3 ± 2.2		6.6 (93.4% passing)

[i.e., absolute value of (calculated dose − averaged measured dose)/averaged measured dose × 100%] between the measured and predicted values when averaged over all measurement points and all plans was 1.8 ± 1.2%, 1.7 ± 1.2%, and 1.8 ± 1.1% for AAA, AXB_D_m, and AXB_D_w, respectively. For IMRT plans, the average absolute discrepancy was 1.9 ± 1.2%, 1.7 ± 1.1%, and 1.8 ± 1.1% for AAA, AXB_D_m, and AXB_D_w, respectively. For RA plans, it was 1.7 ± 1.3%, 1.7 ± 1.2%, and 1.8 ± 1.2%, respectively. Tables VII and VIII show the verification results in OAR. For IMRT plans, the average absolute discrepancy was 1.9 ± 1.3%, 2.5 ± 1.1%, and 2.5 ± 0.8% for AAA, AXB_D_m, and AXB_D_w, respectively. For RA plans, it was 2.3 ± 0.7%, 1.9 ± 0.4%, and 2.6 ± 0.1%, respectively. Figure 6 summarizes the mean percentage discrepancy [i.e., (predicted dose − measured dose)/measured dose *100%] over all plans and all cases. The TLD results showed acceptable accuracy for both AAA and AXB at the selected points, and did not show any significant difference in the dose calculation accuracy among the three calculation options. Moreover, no significant difference could be observed between the results of IMRT and RA plans.

III.D. Stratified PTV doses for real patients

Table IX summarizes the mean doses to PTV_{GTV} and its different components in air, bone, tissue, the 3 mm tissue adjacent to bone, and the 3 mm tissue adjacent to air averaged separately over the three IMRT and the three RA plans used in Secs. III.A–III.C. Among the three options, AXB_D_m predicted the lowest PTV doses while AXB_D_w predicted the highest PTV doses. For IMRT plans, it can be observed that the mean dose to PTV_{GTV} estimated by AXB_D_m and AXB_D_w compared to AAA was 1.1% lower and 0.6% higher, respectively. The mean doses to all stratified components except PTV_{GTV} in air predicted by AXB_D_m were lower than those predicted by AAA. The amount of dose reduction was highest in bone. It was 1.2% lower for

TABLE IV. The averaged results of the gamma evaluations for film measurement within heterogeneous media of the anthropomorphic phantom.

IMRT	Dose calculation	Percentage of pixels with gamma > 1		Average dose difference within the ROI (%) (calculated data − measured data)
		3 mm/3%	2 mm/2%	%Δ
Case 1	AAA	8.2 ± 3.6	24.2 ± 8.8	3.2 ± 0.5
	AXB_Dm	9.5 ± 3.7	20.9 ± 5.7	2.8 ± 0.4
	AXB_Dw	1.2 ± 1.0	4.5 ± 3.0	0.9 ± 0.4
Case 2	AAA	4.0 ± 4.3	15.7 ± 7.4	2.0 ± 0.9
	AXB_Dm	6.7 ± 2.9	18.9 ± 5.6	1.8 ± 0.9
	AXB_Dw	1.8 ± 2.4	10.7 ± 9.8	0.3 ± 1.0
Case 3	AAA	3.0 ± 1.7	15.4 ± 6.4	2.5 ± 0.5
	AXB_Dm	7.1 ± 2.2	20.7 ± 5.2	2.7 ± 0.4
	AXB_Dw	0.3 ± 0.2	3.1 ± 2.4	0.4 ± 0.4
RA	Dose calculation	Percentage of pixels with gamma > 1		Average dose difference within the ROI (%) (calculated data − measured data)
		3 mm/3%	2 mm/2%	%Δ
Case 1	AAA	1.1 ± 0.5	9.9 ± 4.2	1.4 ± 2.4
	AXB_Dm	4.3 ± 2.9	16.3 ± 6.3	1.9 ± 2.4
	AXB_Dw	0.9 ± 1.6	5.7 ± 9.0	−0.9 ± 2.4
Case 2	AAA	4.2 ± 1.8	17.5 ± 6.7	2.6 ± 1.1
	AXB_Dm	10.1 ± 5.3	22.4 ± 7.2	3.0 ± 1.1
	AXB_Dw	0.5 ± 0.2	4.1 ± 1.3	0.5 ± 1.1
Case 3	AAA	9.1 ± 4.1	25.5 ± 7.7	3.2 ± 0.5
	AXB_Dm	14.7 ± 4.5	32.5 ± 6.5	3.3 ± 2.5
	AXB_Dw	1.6 ± 1.2	9.2 ± 4.3	0.8 ± 0.4
		Overall combined (all IMRT and RA plans)		
		3 mm/3%		Confidence limit, CL (|mean|+ 1.96σ)
	AAA	4.9 ± 3.1		11.0 (89.0% passing)
	AXB_Dm	8.7 ± 3.6		15.8 (84.2% passing)
	AXB_Dw	1.0 ± 0.6		2.2 (97.8% passing)

PTV_{GTV}_tissue, 2.4% lower for PTV_{GTV}_bone, 0.7% lower in tissue adjacent to bone, and 0.5% lower in tissue adjacent to air. On the other hand, the mean doses to all stratified components predicted by AXB_D_w were higher than those predicted by AAA. The amount of increase in the mean dose was highest in bone. It was 1.9% in bone and mostly within 1% for all the other stratified components. The differences in mean doses between AXB_D_m and AXB_D_w were mostly within 2% except for the component in bone, for which a difference of up to 4.3% was found. Very similar results were found for the RA plans.

Figures 7(a)–7(d) show the differential dose volume histograms of the stratified PTV_{GTV} structures calculated using the three different calculation options for the IMRT plan of case 1. They displayed the share of the total volumes in the interested structures receiving a certain dose as a function of equivalent dose intervals. From the spread of dose differences among the three options, it was observed that larger dose differences were found between AXB_D_m and AXB_D_w than those between AAA and AXB_D_m for all components. Besides, larger differences in dose distribution among the three calculation options were found in bone than in tissue. The differences found in the tissue adjacent to bone and air were similar to the rest of the tissue in PTV_{GTV}.

IV. DISCUSSION

Although previous investigations proved that AXB_D_m predicted significantly more accurate doses in and near heterogeneous media from single fields compared to AAA,[6–10] the differences might not be as obvious for clinical IMRT and RA fields. For a single field with the presence of air cavity, AXB predicted lower in-field doses, and higher out-of-field doses near air/tissue interfaces compared to AAA due to the better modeling of lateral electronic disequilibrium effect.[12] When multiple field segments are used, the dose variation due to heterogeneity, especially due to low density media such as air from one single field segment would be compensated by adjacent field segments from the same field direction or other field segments coming from different directions.

The verification of the planar dose distribution adjacent to heterogeneous media by film using the head and neck cube reflected satisfactory results for all the three calculation options. The passing rates of the 3%/3mm criterion were

TABLE V. The TLD results of the anthropomorphic head and shoulder phantom verification measurement for the 12 points at/near heterogeneous interfaces inside the target of IMRT plans.

IMRT plans Position	Measured dose Average (cGy)	Calculated dose (cGy)			abs%diff [a] (calculated data − measured data)		
		AAA	AXB_D_m	AXB_D_w	AAA	AXB_D_m	AXB_D_w
			Case 1				
T1	82.1 ± 1.4	83.8 ± 0.4	82.8 ± 0.6	84.5 ± 0.6	2.1	0.9	2.9
T2	78.1 ± 0.8	80.9 ± 1.4	79.0 ± 1.3	81.7 ± 1.3	3.6	1.2	4.7
T3	93.4 ± 1.1	92.1 ± 0.5	92.7 ± 0.3	93.4 ± 0.3	1.3	0.7	0.0
T4	93.2 ± 1.1	92.4 ± 0.5	93.2 ± 0.3	94.0 ± 0.3	0.9	0.0	0.8
T5	91.3 ± 0.1	93.1 ± 0.5	93.7 ± 0.5	94.6 ± 0.5	2.0	2.7	3.7
T6	91.8 ± 1.0	91.0 ± 0.3	90.9 ± 0.1	91.6 ± 0.1	0.9	1.0	0.2
T7	91.3 ± 1.3	90.7 ± 0.9	90.2 ± 0.9	90.6 ± 0.9	0.6	1.2	0.7
T8	90.3 ± 1.1	91.7 ± 0.5	92.7 ± 0.2	93.3 ± 0.2	1.6	2.7	3.3
T9	88.9 ± 0.9	90.5 ± 0.3	91.7 ± 0.5	92.9 ± 0.5	1.8	3.2	4.5
T10	91.8 ± 2.2	92.6 ± 0.6	92.1 ± 0.7	94.3 ± 0.7	0.9	0.3	2.7
T11	92.6 ± 1.2	94.2 ± 0.5	93.8 ± 0.7	96.0 ± 0.7	1.8	1.4	3.7
T12	87.4 ± 0.5	91.0 ± 0.8	91.6 ± 1.1	92.0 ± 1.1	4.1	4.8	5.3
	Average abs%diff over all points				1.8	1.7	2.7
			Case 2				
T1	99.8 ± 1.1	96.1 ± 0.4	95.4 ± 0.4	97.7 ± 0.4	3.7	4.4	2.1
T2	93.6 ± 0.9	93.4 ± 0.7	92.5 ± 0.8	95.0 ± 0.6	0.2	1.1	1.5
T3	97.8 ± 1.1	95.2 ± 0.3	95.7 ± 0.5	96.2 ± 0.5	2.7	2.1	1.6
T4	97.2 ± 0.6	94.5 ± 0.5	95.5 ± 0.7	96.3 ± 0.6	2.8	1.7	0.9
T5	96.5 ± 0.8	96.2 ± 0.2	96.9 ± 0.4	98.1 ± 0.3	0.3	0.4	1.7
T6	95.8 ± 0.8	93.5 ± 0.2	93.4 ± 0.4	94.2 ± 0.2	2.4	2.5	1.6
T7	95.0 ± 1.8	93.1 ± 0.4	93.6 ± 0.2	94.0 ± 0.3	2.0	1.5	1.0
T8	97.1 ± 0.3	93.6 ± 0.5	94.7 ± 0.3	95.4 ± 0.5	3.6	2.5	1.8
T9	95.0 ± 0.7	94.2 ± 0.2	95.4 ± 0.5	95.7 ± 0.2	0.8	0.5	0.8
T10	99.3 ± 1.1	96.0 ± 0.4	96.4 ± 0.3	98.5 ± 0.4	3.3	2.9	0.8
T11	97.2 ± 0.6	96.0 ± 0.1	95.9 ± 0.3	98.0 ± 0.3	1.2	1.3	0.9
T12	95.2 ± 3.3	95.7 ± 0.7	95.7 ± 1.1	96.1 ± 0.6	0.5	0.5	1.2
	Average abs%diff over all points				1.9	1.8	1.3
			Case 3				
T1	82.7 ± 0.8	82.1 ± 0.4	81.6 ± 0.4	83.1 ± 0.3	0.8	1.4	0.4
T2	80.3 ± 1.1	80.3 ± 0.5	80.2 ± 0.2	81.5 ± 0.3	0.0	0.1	1.5
T3	97.3 ± 1.4	93.4 ± 0.5	93.7 ± 0.7	94.8 ± 0.7	4.0	3.7	2.6
T4	96.1 ± 1.1	92.3 ± 0.5	93.3 ± 0.6	94.0 ± 0.5	4.0	2.9	2.2
T5	96.5 ± 1.1	93.8 ± 0.8	94.9 ± 0.7	95.6 ± 0.8	2.8	1.7	1.0
T6	91.9 ± 1.1	89.2 ± 0.3	89.4 ± 0.5	90.1 ± 0.3	2.9	2.7	1.9
T7	92.6 ± 0.8	92.0 ± 0.2	92.4 ± 0.5	92.8 ± 0.3	0.7	0.3	0.2
T8	94.2 ± 1.7	93.1 ± 0.6	94.1 ± 0.2	95.0 ± 0.5	1.2	0.2	0.8
T9	91.9 ± 0.8	93.6 ± 0.4	94.6 ± 0.3	94.9 ± 0.3	1.9	3.0	3.3
T10	96.2 ± 1.8	93.9 ± 0.3	94.2 ± 0.2	96.1 ± 0.3	2.4	2.1	0.1
T11	93.9 ± 1.1	93.1 ± 0.2	92.9 ± 0.6	94.7 ± 0.2	0.9	1.1	0.8
T12	92.2 ± 0.8	93.2 ± 0.3	92.7 ± 0.6	93.6 ± 0.4	1.1	0.5	1.5
	Average abs%diff over all points				1.9	1.6	1.4

[a]abs%diff = [absolute value of (calculated dose − averaged measured dose)]/averaged measured dose × 100%.

higher than 94% on the axial plane and 92% on the coronal plane for all plans calculated by different calculation methods. Although the differences were small, AXB_D_m showed slightly better agreement with measured dose distributions than the other two options on the axial plane. For the axial plane, the presence of air and bone adjacent to the film affected the doses mostly in terms of lateral electron transport and lateral scatter. This might be because AXB_D_m produced better modeling of lateral dose transport in air compared to AAA, and more accurate calculation of lateral scatter and exit doses from the compact bone than both AAA and AXB_D_w. The effect was slightly different and became more complicated when the dose distribution measured by film was on the coronal plane. Radiation fields coming from different directions affected the doses to the interested interface differently. For example, those anterior and anterior oblique fields passed through air and bone before reaching the interface, while those posterior and posterior oblique fields interacted with the interface before passing through the air and bone. The doses on the interface below air and bone could be

TABLE VI. The TLD results of the anthropomorphic head and shoulder phantom verification measurement for the 12 points at/near heterogeneous interfaces inside the target of RA plans.

RA plans Position	Measured dose Average (cGy)	Calculated dose (cGy)			abs%diff[a] (calculated data − measured data)		
		AAA	AXB_D_m	AXB_D_w	AAA	AXB_D_m	AXB_D_w
			Case 1				
T1	86.4 ± 0.4	85.1 ± 0.3	84.1 ± 0.4	85.4 ± 0.3	1.5	2.6	1.1
T2	85.9 ± 0.2	86.5 ± 0.8	85.4 ± 0.8	86.5 ± 0.7	0.7	0.6	0.7
T3	97.9 ± 0.8	95.4 ± 0.7	96.3 ± 0.7	97.2 ± 0.8	2.5	1.6	0.7
T4	95.5 ± 1.1	91.3 ± 1.4	92.4 ± 1.5	94.0 ± 1.6	4.4	2.7	1.6
T5	93.4 ± 0.7	91.4 ± 1.6	93.7 ± 1.6	93.0 ± 1.8	2.2	1.1	0.5
T6	94.3 ± 1.6	95.7 ± 0.5	95.6 ± 0.5	96.7 ± 0.4	1.5	1.4	2.5
T7	97.7 ± 1.6	96.6 ± 0.4	97.7 ± 0.6	97.7 ± 0.3	1.1	0.0	0.0
T8	98.4 ± 2.4	97.6 ± 0.3	98.8 ± 0.6	99.3 ± 0.1	0.8	0.4	0.9
T9	101.3 ± 0.7	100.0 ± 0.4	102.0 ± 0.8	102.1 ± 0.2	1.3	0.7	0.8
T10	99.7 ± 2.1	98.3 ± 0.2	97.6 ± 0.3	99.6 ± 0.2	1.4	2.1	0.1
T11	107.8 ± 0.9	103.3 ± 0.3	103.0 ± 0.6	105.0 ± 0.3	4.2	4.5	2.6
T12	100.8 ± 1.0	101.0 ± 0.3	101.2 ± 0.9	101.7 ± 0.5	0.2	0.4	0.9
		Average abs%diff over all points			1.8	1.5	1.0
			Case 2				
T1	79.3 ± 0.9	81.1 ± 0.2	79.9 ± 0.2	80.9 ± 0.2	2.1	0.7	2.0
T2	85.0 ± 2.8	84.1 ± 0.3	83.2 ± 0.2	84.2 ± 0.4	1.0	2.1	0.9
T3	96.4 ± 0.9	94.0 ± 1.9	94.3 ± 2.0	95.3 ± 2.0	2.5	2.2	1.2
T4	94.1 ± 2.2	93.9 ± 1.8	94.8 ± 2.0	95.6 ± 1.9	0.2	0.8	1.6
T5	92.9 ± 1.0	95.1 ± 1.4	95.4 ± 1.4	96.0 ± 1.4	2.3	2.7	3.3
T6	90.7 ± 0.7	92.8 ± 0.3	92.3 ± 0.4	93.3 ± 0.4	2.3	1.7	2.8
T7	93.3 ± 0.2	94.4 ± 0.3	94.8 ± 0.6	95.0 ± 0.3	1.2	1.6	1.8
T8	98.4 ± 1.3	95.3 ± 0.5	96.1 ± 0.6	96.7 ± 0.1	3.2	2.4	1.8
T9	94.3 ± 0.7	95.0 ± 0.5	96.8 ± 0.6	96.8 ± 0.3	0.8	2.7	2.7
T10	93.0 ± 1.2	95.1 ± 0.9	93.9 ± 0.7	95.9 ± 0.9	2.3	1.0	3.1
T11	100.5 ± 2.1	98.7 ± 0.8	98.1 ± 1.3	99.8 ± 0.9	1.8	2.4	0.7
T12	97.8 ± 0.4	98.4 ± 0.6	98.7 ± 1.0	99.2 ± 0.9	0.6	0.9	1.5
		Average abs%diff over all points			1.7	1.8	1.9
			Case 3				
T1	82.4 ± 1.9	82.7 ± 0.8	82.1 ± 0.7	82.9 ± 0.9	0.3	0.4	0.6
T2	79.0 ± 1.1	81.9 ± 1.2	80.8 ± 1.3	81.8 ± 1.2	3.7	2.3	3.6
T3	93.9 ± 2.3	94.2 ± 0.2	94.7 ± 0.4	95.6 ± 0.2	0.3	0.9	1.8
T4	96.3 ± 1.1	94.6 ± 0.3	95.6 ± 0.4	96.1 ± 0.4	1.7	0.7	0.2
T5	93.6 ± 1.0	94.3 ± 0.5	95.1 ± 0.6	95.5 ± 0.6	0.7	1.6	2.0
T6	90.7 ± 1.0	92.9 ± 0.3	93.2 ± 0.4	94.2 ± 0.2	2.5	2.8	3.9
T7	91.0 ± 1.5	93.8 ± 0.1	94.6 ± 0.6	94.8 ± 0.2	3.1	3.9	4.2
T8	95.6 ± 0.9	96.3 ± 0.8	97.4 ± 0.4	98.2 ± 0.4	0.8	1.9	2.8
T9	95.0 ± 1.4	95.8 ± 0.4	97.3 ± 0.6	97.3 ± 0.2	0.8	2.4	2.4
T10	96.9 ± 1.0	98.5 ± 0.2	98.1 ± 0.3	100.1 ± 0.1	1.7	1.3	3.3
T11	97.3 ± 1.7	97.5 ± 0.1	96.7 ± 0.6	98.5 ± 0.1	0.2	0.6	1.3
T12	94.9 ± 2.1	98.3 ± 0.3	98.4 ± 0.7	98.8 ± 0.3	3.6	3.7	4.1
		Average abs%diff over all points			1.6	1.9	2.5

[a]abs%diff = [absolute value of (calculated dose − averaged measured dose)]/averaged measured dose × 100%.

affected by secondary build-up and build-down effect, forward and backward scatter, lateral scatter, and beam transmission, depending on the beam direction. This might explain why the comparison results on the coronal plane did not reflect consistently better agreement between AXB_D_m and measured doses as on the axial plane.

The verification of planar dose distribution using the head and neck cube was different from that using the anthropomorphic phantom. For the head and neck cube verification, the position of the interested slice was adjacent to bone and air, but was still situated in a tissue equivalent medium. During dose calculation, AXB_D_m represented doses to the tissue equivalent film and AXB_D_w represented doses to unit density water. Both should be close to each other. The main difference between the two calculation options would be the calculated scattered doses from the adjacent bone and air. On the other hand, for the film experiment performed using the anthropomorphic phantom, the slice of interest was situated directly within the heterogeneous medium of the NP region. Part of the film was sandwiched between bony structures. The

TABLE VII. The TLD results of the anthropomorphic head and shoulder phantom verification measurement for the six points near OAR of IMRT plans.

IMRT plans Position	Measured dose Average (cGy)	Calculated dose (cGy)			abs%diff[a] (calculated data − measured data)		
		AAA	AXB_D_m	AXB_D_w	AAA	AXB_D_m	AXB_D_w
			Case 1				
R1	59.7 ± 0.5	60.0 ± 0.4	60.3 ± 0.5	61.3 ± 0.5	0.5	1.0	2.7
R2	59.9 ± 0.9	60.1 ± 0.5	60.4 ± 0.7	60.8 ± 0.7	0.4	0.9	1.5
R3	55.5 ± 0.2	56.0 ± 1.0	56.2 ± 1.1	57.1 ± 1.1	0.9	1.3	2.9
R4	46.4 ± 0.3	46.5 ± 0.8	45.6 ± 0.7	46.7 ± 0.7	0.2	1.7	0.7
R5	51.3 ± 0.9	51.2 ± 0.9	50.2 ± 0.9	51.6 ± 0.9	0.1	2.1	0.7
R6	41.1 ± 0.3	41.1 ± 0.7	40.6 ± 0.8	41.6 ± 0.8	0.1	1.4	1.1
	Average abs%diff over all points				0.4	1.4	1.6
			Case 2				
R1	39.0 ± 0.9	37.7 ± 0.4	37.4 ± 0.6	38.0 ± 0.3	3.2	4.0	2.4
R2	36.0 ± 0.3	34.7 ± 0.6	34.1 ± 0.6	34.6 ± 0.7	3.6	5.2	3.9
R3	38.0 ± 0.3	37.4 ± 0.9	37.0 ± 0.9	37.5 ± 1.0	1.5	2.6	1.3
R4	56.7 ± 0.4	54.8 ± 2.3	53.6 ± 2.4	55.0 ± 2.4	3.4	5.5	3.0
R5	37.7 ± 0.5	39.0 ± 1.0	38.5 ± 0.8	39.1 ± 0.9	3.4	2.1	3.6
R6	42.2 ± 0.5	43.3 ± 0.5	43.1 ± 0.4	43.9 ± 0.4	2.6	2.1	4.0
	Average abs%diff over all points				2.9	3.6	3.0
			Case 3				
R1	43.3 ± 0.3	43.1 ± 0.3	42.7 ± 0.2	43.2 ± 0.3	0.5	1.5	0.3
R2	43.7 ± 0.2	45.3 ± 0.5	45.0 ± 0.5	45.5 ± 0.5	3.6	2.9	4.1
R3	49.0 ± 1.5	51.0 ± 1.1	51.0 ± 1.2	51.5 ± 1.2	4.1	4.1	5.1
R4	41.1 ± 0.8	40.8 ± 0.9	40.5 ± 0.7	41.2 ± 0.7	0.8	1.6	0.1
R5	41.1 ± 0.2	43.0 ± 0.6	42.6 ± 0.6	43.4 ± 0.7	4.5	3.5	5.5
R6	40.1 ± 0.7	40.1 ± 0.3	39.6 ± 0.4	40.3 ± 0.4	0.0	1.3	0.5
	Average abs%diff over all points				2.4	2.5	2.8

[a]abs%diff = [absolute value of (calculated dose − averaged measured dose)]/averaged measured dose × 100%.

presence of bone material within the NP region did make a difference between dose-to-water and dose-to-medium calculation. The bone was different from water in both density and atomic number. For example, a stopping power ratio of water to cortical bone of up to 1.1 could be used to convert dose-to-medium to dose-to-water in the medium. Direct CT simulation of the thin film (0.2 mm) within the NP region was not possible, as it was not practical to perform CT scan of such a thin film with 1.25 mm slice thickness (the smallest slice thickness available for our CT scanner). Therefore, the dose distribution at the selected plane calculated by AXB_D_m should only reflect the doses to bone, air, and tissue within the NP region. Since the EBT3 film itself was tissue-equivalent, its measurement actually represented doses in a medium close to water density in the selected plane. The EBT3 film measured doses should therefore be compared to those calculated by AXB_D_w instead of AXB_D_m. This issue was discussed by Wilcox and Daskalov[19] and Siebers *et al.*[20] using Monte Carlo simulations. AAA computed and reported the absorbed dose as if it were deposited in water, not in medium. The doses predicted by AAA should be directly compared to film. Based on the above argument, we conclude from our investigation

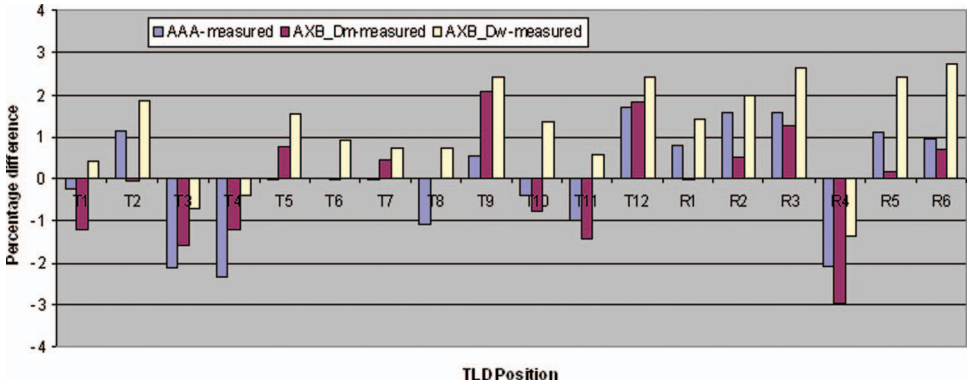

FIG. 6. The percentage dose difference (%diff) between calculated doses and TLD measured doses averaged over all plans for the 18 points selected in the anthropomorphic head and shoulder phantom.

TABLE VIII. The TLD results of the anthropomorphic head and shoulder phantom verification measurement for the six points near OAR of RA plans.

RA plans Position	Measured dose Average (cGy)	Calculated dose (cGy)			abs%diff[a] (calculated data − measured data)		
		AAA	AXB_D_m	AXB_D_w	AAA	AXB_D_m	AXB_D_w
				Case 1			
R1	64.9 ± 0.2	66.6 ± 0.8	66.8 ± 0.7	67.4 ± 0.9	2.5	2.8	3.8
R2	59.3 ± 0.1	60.3 ± 0.3	59.7 ± 0.4	60.4 ± 0.3	1.8	0.7	1.9
R3	60.5 ± 0.6	62.8 ± 0.8	62.4 ± 0.9	63.2 ± 0.7	3.7	3.1	4.4
R4	56.7 ± 0.7	54.3 ± 0.8	54.1 ± 0.9	54.5 ± 0.7	4.2	4.5	3.8
R5	47.4 ± 0.5	47.8 ± 0.6	47.3 ± 0.6	47.8 ± 0.6	0.9	0.2	0.9
R6	48.6 ± 0.5	50.2 ± 0.7	50.2 ± 0.8	50.6 ± 0.7	3.3	3.3	4.1
	Average abs%diff over all points				2.1	2.2	2.7
				Case 2			
R1	45.4 ± 0.2	45.7 ± 0.9	44.9 ± 0.8	45.8 ± 0.9	0.7	1.1	0.9
R2	41.3 ± 1.3	42.2 ± 0.9	41.4 ± 0.9	42.9 ± 0.9	2.1	0.2	3.8
R3	49.9 ± 0.3	49.6 ± 1.1	49.7 ± 1.1	50.4 ± 1.1	0.5	0.3	1.1
R4	57.7 ± 1.1	57.2 ± 1.7	56.3 ± 1.6	57.2 ± 1.7	0.8	2.4	0.8
R5	47.4 ± 1.5	47.7 ± 1.0	47.2 ± 1.1	48.4 ± 1.1	0.7	0.4	2.1
R6	46.8 ± 1.0	48.5 ± 0.9	47.7 ± 1.0	49.0 ± 0.9	3.7	2.0	4.8
	Average abs%diff over all points				1.8	1.5	2.6
				Case 3			
R1	34.8 ± 0.4	36.5 ± 0.4	35.7 ± 0.5	36.2 ± 0.5	4.9	2.6	4.0
R2	43.4 ± 0.4	45.7 ± 0.8	44.9 ± 0.8	45.3 ± 0.8	5.3	3.5	4.4
R3	50.9 ± 0.2	52.3 ± 1.1	51.9 ± 1.2	52.8 ± 1.1	2.7	1.9	3.7
R4	50.0 ± 0.6	48.3 ± 0.9	48.9 ± 0.9	49.4 ± 0.9	3.4	2.2	1.2
R5	49.0 ± 1.1	47.7 ± 1.0	48.1 ± 1.0	49.8 ± 1.0	2.7	1.9	1.6
R6	57.4 ± 1.2	55.3 ± 1.5	57.1 ± 1.3	58.6 ± 1.6	3.7	0.6	2.1
	Average abs%diff over all points				3.1	2.1	2.5

[a]abs%diff = [absolute value of (calculated dose − averaged measured dose)]/averaged measured dose × 100%.

that AXB would predict more accurate dose distribution when compared to AAA near the NP region based on the verification by film.

Measurement by TLD chips was used by the authors as an alternative method for dose verification. The advantages of using film for verification were provision of very good spatial resolution and the involvement of a massive number of points in a single measurement. When compared to film verification, the advantages of using TLD included the verification of doses at specific points of interest and the allowance

TABLE IX. The mean doses to PTV_{GTV} and its different components in air, bone, tissue, the 3 mm tissue adjacent to bone and the 3 mm tissue adjacent to air averaged separately over the three IMRT plans and the three RA plans.

	Mean dose (cGy)			%diff[a]	
IMRT plans	AAA	AXB_D_m	AXB_D_w	AXB_D_m−AAA	AXB_D_w−AAA
PTV_{GTV}	7220 ± 30	7150 ± 30	7270 ± 20	−1.1	0.6
PTV_{GTV}_tissue	7230 ± 30	7150 ± 40	7240 ± 40	−1.2	0.1
PTV_{GTV}_bone	7230 ± 10	7060 ± 10	7360 ± 20	−2.4	1.9
PTV_{GTV}_air	7190 ± 20	7280 ± 50	7270 ± 40	1.2	1.1
PTV_{GTV}_adj bone	7230 ± 10	7170 ± 20	7300 ± 20	−0.7	1.0
PTV_{GTV}_adj air	7230 ± 20	7200 ± 40	7280 ± 50	−0.5	0.7
	Mean dose			%diff[a]	
RA plans	AAA	AXB_D_m	AXB_D_w	AXB_D_m−AAA	AXB_D_w−AAA
PTV_{GTV}	7220 ± 10	7140 ± 20	7250 ± 10	−1.2	0.4
PTV_{GTV}_tissue	7230 ± 10	7130 ± 10	7230 ± 10	−1.4	0.0
PTV_{GTV}_bone	7210 ± 20	7040 ± 20	7330 ± 30	−2.4	1.7
PTV_{GTV}_air	7200 ± 30	7270 ± 20	7260 ± 20	1.0	0.8
PTV_{GTV}_adj bone	7230 ± 20	7150 ± 30	7290 ± 20	−1.1	0.8
PTV_{GTV}_adj air	7240 ± 10	7180 ± 10	7270 ± 20	−0.8	0.4

[a]%diff = (mean dose calculated by AXB_D_m or AXB_D_w − mean dose calculated by AAA)/ mean dose calculated by AAA × 100%.

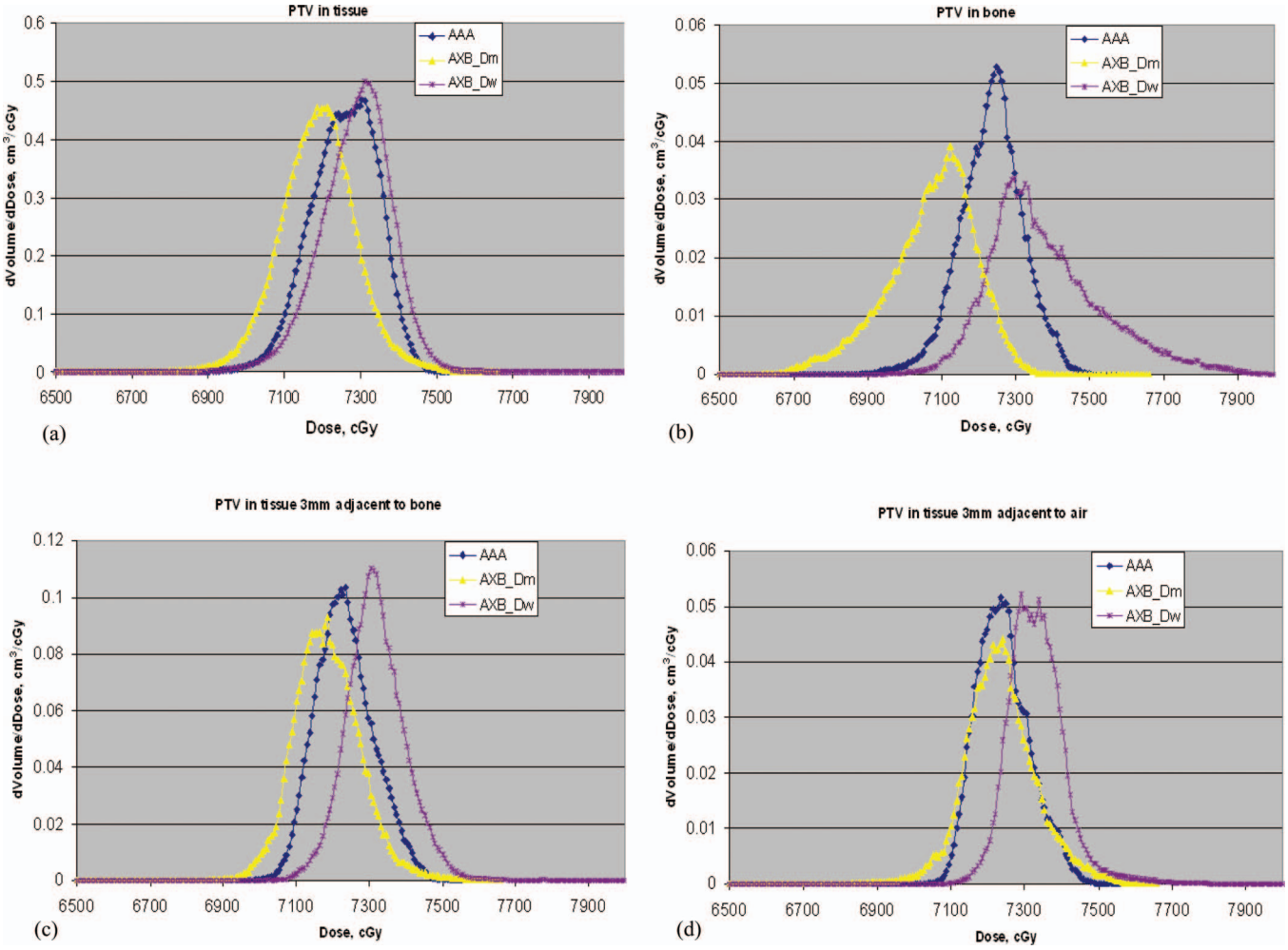

FIG. 7. The differential DVH of (a) PTV_{GTV}_tissues, (b) PTV_{GTV}_bone, (c) PTV_{GTV}_adj bone, and (d) PTV_{GTV}_adj air structures calculated using the three different calculation options for the IMRT plan of case 1.

of different beam orientations relative to the detectors. The verification of point doses with TLDs in this study could not distinguish the accuracy among the calculation options. The estimated dose values by AAA, AXB_D_m, and AXB_D_w were listed in Tables V–VIII for the selected points, the uncertainties listed for the algorithms were the dose variations within the contoured volumes of the TLD chips, which were mostly about 1% in the target and 2%–3% in OAR outside the target. As can be seen from the tables, although there were differences among the calculated doses by the three calculation options, they were mostly about 1%–2%. The precision of the TLD measurement was about 2%–3%. Therefore, the TLD measurement could not distinguish the accuracy difference among AAA, AXB_D_m, and AXB_D_w. However, from this experiment, the authors could at least ensure that the discrepancies between the measured values and predicted values were within acceptable limit for AAA and AXB at/near the heterogeneous interfaces.

The amount of dose variation due to air cavity strongly depends on the field size. The effect of lateral electronic equilibrium increases as the field size decreases. In our previous study, verification by TLD using stereotactic IMRT fields for persistent NPC showed significant improvement in the dose accuracy using AXB.[12] For IMRT and RA fields of primary NPC, the sizes of field segments were larger than those for stereotactic radiotherapy boost due to the need of irradiating much larger target volumes. Besides, the materials passed by the irradiating fields are also different. For example, compared to persistent NPC, the target volume of primary NPC involved more bone content. Therefore, the amount of improvement of dose calculation accuracy demonstrated by AXB compared to that of AAA observed in the current study was less significant.

From the result of the PTV dose analysis in real patients, it was observed that the discrepancies in doses calculated in bone among the three calculated options were larger than those in air, adjacent tissue, and the other remaining tissues. It was within 2% in tissue adjacent to bone and air, and could be about 4% in bone. This matched with the verification results where significant difference in the dose calculation accuracy between AAA and AXB was not found. AAA computes the transport and dose deposition using radiological and density scaling. It computed and reported the absorbed dose as if it were deposited in water. Both options of AXB

calculated dose considering the elemental composition of bony structures. Doses calculated using AXB_D_w was generated by converting the doses calculated by AXB_D_m with the stopping power ratio for water to the specific medium. The stopping power ratio of water to bone is about 1.03 for soft bone and 1.1 for cortical bone. As a result, AXB_D_m computed a lower dose within bony structure than AXB_D_w. Previous investigations showed that the doses calculated by AXB_D_m in bone matched well with those predicted by Monte Carlo simulations.[8–10]

It was also found that the doses calculated by AAA in bone were closer to AXB_D_m than to AXB_D_w. A previous study using Monte Carlo calculations proved that conventional photon dose calculation using water with relative electron densities produced dose distributions in bone were much closer to D_m distributions than to D_w distributions for high-energy (4–18 MV) photon beams. They therefore suggested to use D_m in Monte Carlo photon algorithms for consistency with previous radiation therapy experience, and stated that their recommendations should be applicable to other deterministic dose algorithms or other model-based algorithms.[21] According to the recommendation of AAPM report 105, algorithms taking into account the elemental compositions of materials for dose calculations should provide both dose-to-medium and dose-to-water options for users.[22] There are a few arguments for using the D_w options: (1) Conventional dose algorithms compute and report the absorbed dose as if it were deposited in water. (2) Beam data are always measured in water for the commissioning of the treatment planning system. (3) Absorbed dose-to-water based ionization chamber calibration protocols are used for treatment machines, and (4) tumor cells even when embedded in bone behave like water. Since these two options are available in AXB for the users to select, it is very important for them to be aware that using AXB_D_w will calculate up to 4% more mean doses to the PTV in bone, and up to about 2% more mean doses to the tissues adjacent to bone compared to AXB_D_m for IMRT and RA of NPC. Slightly higher doses to the nearby tissues predicted by AXB_D_w might be due to the larger exit and scattered doses from bone. A previous study using Monte Carlo method also showed dose differences of up to 5.8% in target between D_m and D_w calculations for head and neck cases.[23] Our study using stratified components clearly showed that the dose differences in bone between D_w and D_m were larger than those in the other tissues. The observation from our results could also apply to the IMRT and RA of other head and neck cases.

V. CONCLUSION

The experimental validation study using the anthropomorphic phantom by TLD showed both AAA and AXB produced acceptable accuracy for dose calculation adjacent to heterogeneous media for IMRT and RA plans of NPC. The planar dose verifications using film showed that AXB produced slightly better or equivalent accuracy compared to AAA adjacent to and within the heterogeneous medium. Users using the AXB algorithm for improving dose calculation accuracy should be aware of the dose differences in target volumes between options of D_m and D_w. It should be noted that dose predicted by D_w is usually higher than that predicted by the D_m option, especially in bone and tissues adjacent to bone.

[a]Author to whom correspondence should be addressed. Electronic mail: kanwkm@ha.org.hk; Telephone: (852) 2990-2776; Fax: (852) 2990-2775.

[1]M. Guckenberger, A. Richter, T. Krieger, J. Wilbert, K. Baier, and M. Flentje, "Is a single arc sufficient in volumetric-modulated arc therapy (VMAT) for complex-shaped target volumes?," Radiother. Oncol. **93**, 259–265 (2009).
[2]W. Verbakel, J. P. Cuijpers, D. Hoffmans, M. Bieker, B. Slotman, and S. Senan, "Volumetric intensity-modulated arc therapy vs conventional IMRT in head-and-neck cancer: A comparative planning and dosimetric study," Int. J. Radiat. Oncol., Biol., Phys. **74**, 252–259 (2009).
[3]P. Doornaert, W. Verbakel, M. Bieker, B. Slotman, and S. Senan, "RapidArc planning and delivery in patients with locally advanced head and neck cancer undergoing chemoradiotherapy," Int. J. Radiat. Oncol., Biol., Phys. **79**, 429–435 (2011).
[4]M. K. Kam, R. M. Chau, J. Suen, P. H. Choi, and P. M. Teo, "Intensity-modulated radiotherapy in nasopharyngeal carcinoma: Dosimetric advantage over conventional plans and feasibility of dose escalation," Int. J. Radiat. Oncol., Biol., Phys. **56**, 145–157 (2003).
[5]S. L. Wolden, W. C. Chen, D. G. Pfister, D. H. Kraus, S. L. Berry, and M. J. Zelefsky, "Intensity-modulated radiation therapy (IMRT) for nasopharynx cancer: Update of the Memorial Sloan-Kettering experience," Int. J. Radiat. Oncol., Biol., Phys. **64**, 57–62 (2006).
[6]O. N. Vassiliev, T. Wareing, J. McGhee, G. Failla, M. Salehpour, and F. Mourtada, "Validation of a new grid based Blotzmann equation solver for dose calculation in radiotherapy with photon beams," Phys. Med. Biol. **55**, 581–598 (2010).
[7]A. Fogliata, G. Nicolini, A. Clivio, E. Vanetti, P. Mancosu, and L. Cozzi, "Dosimetric validation of the Acuros XB advanced dose calculation algorithm: Fundamental characterization in water," Phys. Med. Biol. **56**, 1879–1904 (2011).
[8]A. Fogliata, G. Nicolini, A. Clivio, E. Vanetti, and L. Cozzi, "Dosimetric evaluation of Acuros XB Advanced Dose Calculation algorithm in heterogeneous media," Radiat. Oncol. **6** (2011).
[9]K. Bush, I. M. Gagne, S. Zavgorodni, W. Ansbacher, and W. Beckham, "Dosimetric validation of Acuros XB with Monte Carlo methods for photon dose calculations," Med. Phys. **38**, 2208–2221 (2011).
[10]T. Han, J. Mikell, M. Salehpour, and F. Mourtada, "Dosimetric comparison of Acuros XB deterministic radiation transport method with Monte Carlo and model-based convolution methods in heterogeneous media," Med. Phys. **38**, 2651–2664 (2011).
[11]T. Han, F. Mourtada, K. Kisling, J. Mikell, D. Followill, and R. Howell, "Experimental validation of deterministic Acuros XB algorithm for IMRT and VMAT dose calculations with the Radiological Physics Center's head and neck phantom," Med. Phys. **39**, 2193–2202 (2012).
[12]W. K. Kan, L. Leung, and P. Yu, "Verification and dosimetric impact of Acuros XB algorithm on intensity modulated stereotactic radiotherapy for locally persistent nasopharyngeal carcinoma," Med. Phys. **39**, 4705–4714 (2012).
[13]W. Ulmer, J. Pyyry, and W. Kaissl, "A 3D photon superposition/convolution algorithm and its foundation on results of Monte Carlo calculations," Phys. Med. Biol. **50**, 1767–1790 (2005).
[14]A. Fogliata, G. Nicolini, E. Vanetti, A. Clivio, and L. Cozzi, "Dosimetric validation of the anisotropic analytical algorithm for photon dose calculation: Fundamental characterization in water," Phys. Med. Biol. **51**, 1421–1438 (2006).
[15]International Commission on Radiological Protection, "Anatomical, physiological and metabolic characteristics: Reference manual," International Commission on Radiological Protection Report No. 23 (ICRP, New York, 1975).
[16]G. A. Ezzell, J. W. Burmeister, N. Dogan, T. J. LoSasso, J. G. Mechalakos, D. Mihailidis, A. Molineu, J. R. Palta, C. R. Ramsey, B. J. Salter, J. Shi, P. Xia, N. J. Yue, and Y. Xiao, "IMRT commissioning: Multiple institution planning and dosimetry comparisons, a report from AAPM Task Group 119," Med. Phys. **36**, 5359–5373 (2009).
[17]D. Low, J. Dempsey, R. Venkatesan, S. Mutic, J. Markman, E. Haacke, and J. Purdy, "Evaluation of polymer gels and MRI as a 3-D dosimeter for intensity-modulated radiation therapy," Med. Phys. **26**, 1542–1551 (1999).

[18]J. L. Bedford, P. J. Childs, V. N. Hansen, M. A. Mosleh-Shirazi, F. Verhaegen, and A. P. Warrington, "Commissioning and quality assurance of the Pinnacle radiotherapy treatment planning system for external beam photons," Br. J. Radiol. **76**, 163–176 (2003).
[19]E. Wilcox and G. Daskalov, "Accuracy of dose measurements and calculations within and beyond heterogeneous tissues for 6 MV fields smaller than 4 cm produced by Cyberknife," Med. Phys. **35**, 2259–2266 (2008).
[20]J. V. Siebers, P. J. Keall, A. E. Nahum, and R. Mohan, "Converting absorbed dose to medium to absorbed dose to water for Monte Carlo based photon beam dose calculations," Phys. Med. Biol. **45**, 983–995 (2000).
[21]C. M. Ma and J. Li, "Dose specification for radiation therapy: Dose to water or dose to medium?," Phys. Med. Biol. **56**, 3073–3089 (2011).
[22]I. J. Chetty, B. Curran, J. E. Cygler, J. J. DeMarco, G. Ezzel, B. A. Faddegon, I. Kawrakow, P. J. Keall, H. Liu, C. M. Ma, D. W. O. Rogers, J. Seuntjens, D. Sheikh-Bagheri, and J. V. Siebers, "Report of the AAPM Task Group No. 105: Issues associated with clinical implementation of Monte Carlo-based photon and electron external beam treatment planning," Med. Phys. **34**, 4818–4853 (2007).
[23]N. Dogan, J. V. Siebers, and P. J. Keall, "Clinical comparison of head and neck and prostate IMRT plans using absorbed dose to medium and absorbed dose to water," Phys. Med. Biol. **51**, 4967–4980 (2006).